Quantitative ATR-IR Analysis of Anisotropic Polymer Films: Surface Structure of Commercial PET

Kiril R. Kirov and Hazel E. Assender*

Department of Materials, University of Oxford, Parks Road, Oxford OX1 3PH, U.K.

Received March 8, 2005; Revised Manuscript Received August 29, 2005

ABSTRACT: A commercial PET film has been characterized using variable-angle ATR-IR spectroscopy to create a depth profile of the surface. The anisotropic optical constants (n, k) of the film were extracted from the reflectivity spectra assuming that the depth region probed at each angle of incidence is homogeneous. The refractive index n, absorption index k, and absorption coefficient K spectra of the film were then employed to calculate the *trans*/*gauche* content of PET and the extent of *trans* conformer orientation as a function of depth of penetration. The *trans*-PET content of the commercial film we analyzed changes from 78% at a depth of penetration of 0.4 μm to 61% at a depth of penetration of 1.1 μm. Results of the orientational analysis of the film are presented, and problems specific to ATR-IR spectroscopy in such analysis are also discussed.

Introduction

In a previous paper[1] we outlined the methodology used for quantitative ATR-IR analysis of anisotropic polymer films with orthorhombic symmetry in their optical properties and presented results of the first stage of the analysis—the extraction of the optical constants (n, k) of such films. The present paper focuses on the second stage of the analysis—the estimation of the degree of molecular orientation and crystallinity of polymer films using the intensity of bands in the derived spectra.

We use ATR-IR spectroscopy to investigate the surface structure of poly(ethylene terephthalate) (PET) films formed by drawing. PET films are important with more than 50 specific applications, including the production of photographic films, magnetic media, flexible packaging, wire and cable insulators, etc.[2] The packaging applications of PET are diverse and range from foils for food wrapping to thermoforming trays, beverage bottles, and packaging of medical products and electronic devices. More recently, there has also been interest in using PET films as flexible substrates in the manufacturing of light-emitting diodes and photovoltaic devices.[3,4]

Obtaining quantitative information on the surface structure of PET films and sheets is of interest not only due to the commercial importance of their surface properties but also because there is evidence of structural variation in the surface region. Starting with thick (3 mm) PET sheets formed by injection molding, two studies have found evidence for the existence of a thin mainly amorphous skin (600−750 μm thick) and a crystalline core in such sheets.[5,6] The skin−core morphology in injection-molded PET has a thermal origin—the development of crystallinity is impeded at the cool wall of the mold.

At the opposite end of the film thickness scale, a combination of XPS and reflection−absorption infrared spectroscopy has revealed a difference in the rate of crystallization at the surface (top 5 nm) and in the bulk of a 150 nm thick PET film formed by spin-casting on silicon.[7] The observed kinetic difference was attributed to the enhanced molecular mobility at the surface of polymer films in accord with a suggestion made by Keddie, Jones, and Cory[8] on the basis of T_g reduction in thin PMMA and polystyrene films. The experimental data gathered by Hayes et al. also lead the authors to suggest that the surface layer of the spin-cast PET film has attained a greater degree of crystallinity than the film interior.[7]

Evidence for stratification has also been found in drawn PET films.[9−11] The Raman spectra obtained by Everall et al.[9] showed differences in the content of the *trans*-glycol conformer when scanning a microprobe along the thickness direction of a 150 μm thick PET film formed by stretching along one direction.

The drawing of an amorphous 200 μm thick PET film to draw ratios greater than two at 90 °C and a rate of 1000%/min also resulted in the formation of structural gradients.[10] Walls and Coburn used s-polarized light ATR-IR measurements to probe the surface of the drawn PET films on a scale 0.5−5 μm. Their results indicated an increase in the content and in the orientation of the *trans*-PET conformer closer to the film surface. The formation of structural gradients was associated with the evolution of heat due to energy dissipation during stretching, which as a result of the slow heat transfer with the film surroundings leads to temperature variations inside the drawn PET films.

While Walls and Coburn's evidence of stratification in drawn PET films is interesting, it has the shortcoming of being qualitative in nature. In addition, the increase in *trans*-PET conformer content closer to the film surface inferred by them has an element of uncertainty due to the fact that their s-polarized data are only representative of changes in trans conformer concentration in the film plane. Our objective is to obtain quantitative information on surface structure variation in oriented PET films using a methodologically more rigorous method for spectroscopic analysis. In the present paper we aim to verify the existence of structural gradients in a commercial PET film that was

* Corresponding author: Tel +44-(0)1865-273781; Fax +44-(0)-1865-273789; e-mail hazel.assender@materials.ox.ac.uk.

10.1021/ma050495i CCC: $30.25
Published on Web 10/08/2005

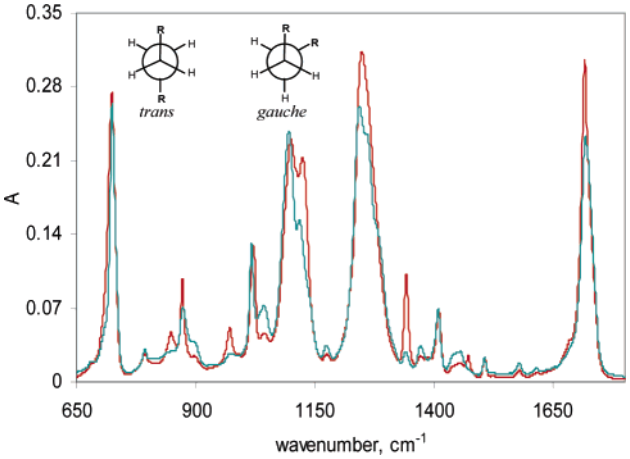

Figure 1. ATR-IR spectra of amorphous (green line) and semicrystalline (red line) PET. Inset: *trans*- and *gauche*-ethylene glycol conformers.

Table 1. Spectral Assignments of Absorption Bands in the Infrared Spectrum of PET Commonly Used for *Trans/Gauche* Concentration Analysis and for Analysis of Molecular Orientation[a]

$\bar{\nu}$, cm^{-1}	mode of vibration	θ_m, deg
1410[38]	ring C−C stretching ν'_{13} (B_{2u}), reference band	
1370[12]	γ_w (CH_2) (*gauche*)	
1340[12]	γ_w (CH_2) (*trans*)	21[37]
1019[38]	CH in-plane deformation ν_{18A} (B_{2u})	20[22]
971[12]	*A* (*trans*)[12] or γ_r (CH_2)[13] (*trans*)	34[37]
896[13]	γ_r (CH_2) (*gauche*)	
875[38]	CH out-of-plane deformation ν_{17B} (B_{1u})	85[39]

[a] θ_m = angle between the transition moment vector of the vibration and the chain axis, *A* = vibration of the −O−CH_2−CH_2−O− group, ν = bond stretching, γ_w = wagging vibration, and γ_r = rocking vibration.

formed via the flat-film production method. An investigation of surface structure development in PET films during drawing will be presented in a future publication.

Methodology

***Trans/Gauche* Analysis of PET.** The infrared spectra of amorphous and semicrystalline PET show distinct differences (Figure 1). The origin of these differences has been a matter of much debate, but at present the idea put forward by Grime and Ward[12] has been universally accepted. Grime and Ward suggested that the differences are due to rotational isomerism in the ethylene glycol residue of PET. In particular, the bands positioned at 1470, 1340, 975, and 845 cm^{-1} arise from vibrations of the *trans*-ethylene glycol (EG) conformer. The bands located at 1450, 1370, 1040, and 898 cm^{-1} are due to vibrations of the *gauche* conformer. Table 1 presents the spectral assignments of the infrared bands most often used for analysis of *trans*/*gauche* concentration and molecular orientation in PET.

The *trans*/*gauche* EG content of PET can be estimated using the following expression:[5]

$$a_{trans}\frac{I_{trans}}{I_{ref}} + b_{gauche}\frac{I_{gauche}}{I_{ref}} = 1 \qquad (1)$$

In (1) we employ the intensities of the 1340, 1370, and 1410 cm^{-1} bands in the averaged absorption coefficient spectrum $K_0 = {}^1/_3(K_x + K_y + K_z)$ of PET, K_x, K_y, and K_z being the principal components of the anisotropic absorption coefficient spectrum. Multiplication of (1) by I_{ref}/I_{trans} yields

$$a_{trans} + b_{gauche}\frac{I_{gauche}}{I_{trans}} = \frac{I_{ref}}{I_{trans}} \qquad (2)$$

and therefore the *trans* and *gauche* weight coefficients (a_{trans}, b_{gauche}) can be found from the linear plot of I_{ref}/I_{trans} against I_{gauche}/I_{trans}.

Several studies have reported good correlation between the *trans*-EG conformer content and the degree of crystallinty of PET.[5,13,14] The correlation is based on the fact that chains in the crystalline unit cell of PET are in an extended *all-trans* conformation. No *gauche* conformer is therefore to be found in the crystalline domains of semicrystalline PET. Recent investigations of the crystallization mechanism of PET have concluded that it is preceded by spinodal decomposition of the polymer melt from the *gauche* conformation into regions rich in *trans* and *gauche* conformers before crystalline (interchain) ordering occurs.[15−21] Consequently, the *trans*-EG conformer can be present both in the crystalline and in the amorphous phase, the exact proportions depending on the treatment of the polymer.[13] Quantanilla et al., however, have shown that upon heat treatment of isotropic PET the concentration of the *trans*-EG conformer present in the amorphous phase decreases quickly and vanishes at a treatment temperature higher than 110 °C.[5]

Commercial PET films pass through a heat-setting operation during their manufacturing process, which is usually conducted in the range 150−240 °C.[2] Since the film we are analyzing in this work is a commercial film, it is plausible to assume that the *trans*-EG unit is predominantly located in the crystalline phase of the film. *Trans/gauche*-EG concentration estimates obtained using infrared spectroscopy can therefore serve as useful indicators of the phase composition of the film.

Infrared Orientational Analysis. The method for quantitative orientational analysis followed here has been developed by Cunningham et al.[22] and Jarvis et al.[23] in a manner similar to the approach used for description of crystallite orientation in polycrystalline materials using X-ray diffraction.[24] The polymer sample is considered to be an aggregate of noninteracting anisotropic structural units of orthorhombic symmetry. Three Euler angles (θ, ϕ, ψ) define the orientation of an orthogonal set of axes (*abc*) fixed in the microscopic structural unit with respect to the reference macroscopic coordinate system (*xyz*) (Figure 2a). Expanding the most probable distribution function $N(\theta,\phi,\psi)$ of the microscopic structural units into a series of spherical harmonics yields the orientation average coefficients P_{lmn}.[25] The P_{lmn} coefficients assume a value of 1 for perfect orientation of the microscopic structural unit along a particular macroscopic axis, −0.5 for perpendicular orientation and 0 for no preferential orientation.

The molecular orientation parameters P_{lmn} are calculated from infrared spectroscopic data in the following manner. First, the principal polarizabilities of a unit volume of the material ϕ_i ($i = x, y, z$) are calculated using the refraction n and absorption index k data for a particular infrared vibration[22]

$$\phi_i = 6n_ik_i\{(n_i^2 + 2)^2 + (2n_i^2 - 4)k_i^2 + k_i^4\}^{-1} \qquad (3)$$

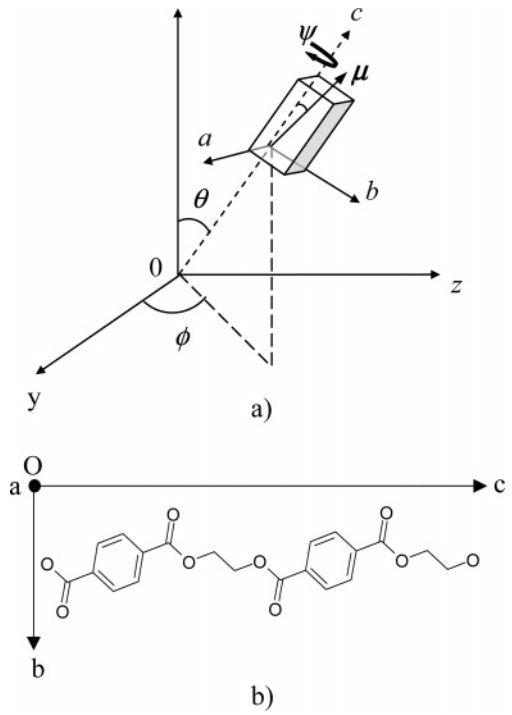

Figure 2. Definition of reference coordinate axes: (a) the Euler angles θ, ϕ, and ψ, which specify the orientation of a molecular coordinate system (*abc*) with respect to a macroscopic Cartesian axis system (*xyz*); (b) the microscopic axes *a*, *b*, and *c* in the *all-trans* PET unit.

For a sample with a general biaxial statistical symmetry, ϕ_i and the four P_{lmn} coefficients that can be derived from infrared spectroscopy are related via eqs 4[23]

$$\frac{2\phi_x - \phi_y - \phi_z}{\phi_x + \phi_y + \phi_z} = 2p_{200}(\theta_m)P_{200} + 4p_{200}(\theta_m)P_{202} - 4P_{202}$$

$$\frac{\phi_y - \phi_z}{\phi_x + \phi_y + \phi_z} = 4p_{200}(\theta_m)P_{220} + \frac{4}{3}p_{200}(\theta_m)P_{222} - \frac{4}{3}P_{222} \quad (4)$$

The constant $p_{200}(\theta_m) = {}^1/_2(3\cos^2\theta_m - 1)$ in (4) is determined by the angle θ_m, which the molecular dipole moment μ makes with the chain axis. From (4) it follows that in order to calculate all four P_{lmn} coefficients it is necessary to use for the analysis the (n, k) parameters of two absorption bands with known θ_m and solve a system of four equations.

The P_{lmn} coefficients can be further transformed into average squared direction cosines.[23] The direction cosines have the advantage of being more straightforward to interpret—for random orientation they assume a value of ${}^1/_3$, perfect orientation along an axis is characterized by a value of 1, whereas no orientation leads to a value of 0.

Here, we analyze the orientation of the *trans*-EG segment and of the benzene ring of PET relative to the macroscopic film directions *x*, *y*, and *z*. The analysis is carried out using the intensity of the following dichroic absorption bands: 1340 and 971 cm^{-1} for the *trans*-EG conformer and 1019 and 875 cm^{-1} for the benzene ring. Following our previous work,[1] the direction of preferred chain orientation in the sample is denoted as *x*; *y* is the direction orthogonal to *x* in the film plane, and *z* is the film thickness direction. Following the assumption that the *trans*-EG conformer in PET-T is predominantly located in the crystalline phase, estimates of the orientation of the latter correspond to the orientation of the PET monomer units in the *all-trans* conformation. Previous investigations have established that the *all-trans* segment is planar[26,27]—the main backbone defines a linear zigzag with the repeat unit being parallel to the end-to-end vector.[28] The set of microscopic reference axes with respect to the *all-trans* unit is defined as follows (Figure 2b): *c* is the long-chain axis direction; *b* and *a* are the two directions orthogonal to *c*, which correspond to the width and thickness of the microscopic structural unit, respectively. With this choice of axes the benzene ring of the terephthalic unit is contained in the *Obc* plane. The same is true for the main C−C bond of the ethylene glycol segment.

Experimental Section

Surface structure analysis using attenuated total reflection infrared (ATR-IR) spectroscopy was performed on a 12 μm thick commercial PET film, here referred to as PET-T. The ATR-IR experiments were carried out on a Perkin-Elmer Spectrum 2000 Explorer FTIR spectrometer equipped with a variable angle reflection attachment (Seagull, Harrick Scientific Corp.). For depth profiling, polarized light ATR-IR measurements were made at seven different angles of incidence along the principal optic axes of the film without breaking the contact between the internal reflection element and the sample. The employed angles of incidence are 28, 30, 32, 36, 40, 44, and 52°.

The bulk degree of crystallinity of PET-T was determined using differential scanning calorimetry according to relation 5:

$$X_c^{DSC} = \frac{\Delta H_f}{\Delta H_{f,0}} \quad (5)$$

where ΔH_f represents the measured heat of fusion of the analyzed polymer and $\Delta H_{f,0}$ is the heat of fusion of a perfect crystal of the same polymer. For PET, the accepted value for $\Delta H_{f,0}$ is 24.1 kJ mol^{-1}.[29] The DSC experiments were carried out on a Perkin-Elmer DSC-7 machine at a heating rate of 10 °C min^{-1} in the interval 30−280 °C while purging the heating cell with nitrogen.

Results and Discussion

The extraction of the optical constants of PET from ATR-IR spectra has been discussed in detail previously.[1] We note that our calculations there assumed light incidence toward the interface between two homogeneous optical media. The same simplified approach is maintained in the depth-profiling analysis of PET-T presented below. For depth profiling, it is more appropriate to follow rigorously the theory of plane wave propagation in stratified media. However, such calculations suffer from increased complexity even for isotropic media and from uncertainties regarding the actual shape of the assumed concentration profile. For the task of verifying the existence of a surface structural variation, the assumption that a homogeneous medium with an effective complex refractive index $\hat{n}_2^{eff}$ and a thickness d_p^{eff} is probed at each angle of incidence is well justified.

***Trans/Gauche* Concentration Analysis.** Figure 3 presents the absorption index spectra k_0 of PET-T obtained over the range of wavenumbers of interest from ATR-IR depth profiling. The calculated spectra are in good agreement with the k_0 standard of PET.[1] There is however some baseline variation in the spectra, which

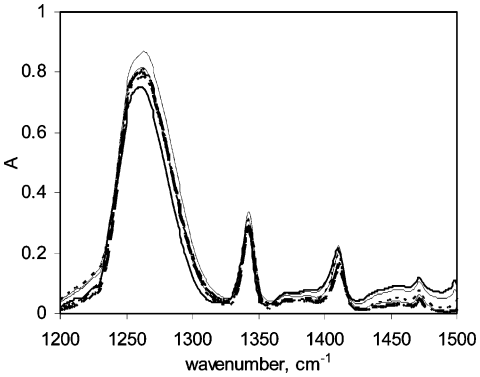

Figure 3. Absorption index spectra k_0 of PET-T obtained from ATR-IR depth profiling.

combined with the low intensity of the 1370 cm^{-1} *gauche* band makes quantitative analysis difficult.

Before presenting the results of the conformational depth profiling for PET-T, we should note that unless the complex refractive index of the analyzed material is available a practicing spectroscopist has no means of a priori knowing the thickness of the layer probed in the ATR-IR experiment. Because of the exponential decay of the electric field into the nonincident medium, the choice of a depth parameter is arbitrary.

Parameters like depth of penetration d_p[30] and sampling depth d_s[31] have been employed. Harrick defined d_p as the distance into the nonincident medium at which the electric field E decays from its initial value E_0 at the ATR crystal/sample interface to a value $E = E_0e^{-1}$. The penetration depth into a nonabsorbing medium is then[30]

$$d_p = \frac{\lambda}{2\pi(n_1^2 \sin^2 \theta_i - n_2^2)^{1/2}} \quad (6)$$

where n_1 and n_2 are the refractive indices of the ATR crystal and of the sample respectively, λ is the wavelength of the incident radiation in free space, and θ_i is the angle of incidence measured from the surface normal. It is straightforward to calculate d_p for a nonabsorbing medium if the refractive index n_2 at a particular wavelength is known. The refractive index of an absorbing medium however is complex, $\hat{n}_2 = n_2 + ik_2$, and the depth of penetration is therefore determined by both the refractive and the absorption properties of the medium.

Figure 4 contains a plot of the depth of penetration into a nonabsorbing medium (dashed line), which has a refractive index of 1.60. For comparison, in the same figure we have plotted the modulus of d_p into PET-T (solid line) calculated using the n_2 and k_2 spectra of PET-T extracted from the reflectivity spectrum of the film measured at an angle of incidence of 36°. The presented $|d_p|$ spectrum is in fact the average of the depths of penetration obtained from the three polarized light measurements required for full characterization of an optically biaxial film, e.g., $|d_p(\hat{n}_2)| = {}^1/_3(|d_p^{TEx}| + |d_p^{TEy}| + |d_p^{TMy}|)$. The calculated depths of penetration at the location of k_{max} for the trio of bands that we have selected for conformational analysis of PET are as follows: $|d_p^{1410}(\hat{n}_2)| = 0.609$ μm, $|d_p^{1370}(\hat{n}_2)| = 0.617$ μm, and $|d_p^{1340}(\hat{n}_2)| = 0.620$ μm. That the obtained d_p values are so similar is very fortunate and confirms the suitability of the three bands for concentration analysis.

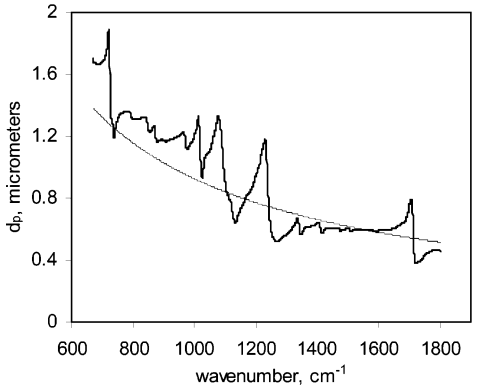

Figure 4. Spectral depth of penetration into a hypothetical nonabsorbing medium (dashed line) and into PET-T (solid line). Experimental ATR-IR parameters: $\theta = 36°$, $n_1 = 4.0$, $n_{2\infty} = 1.60$.

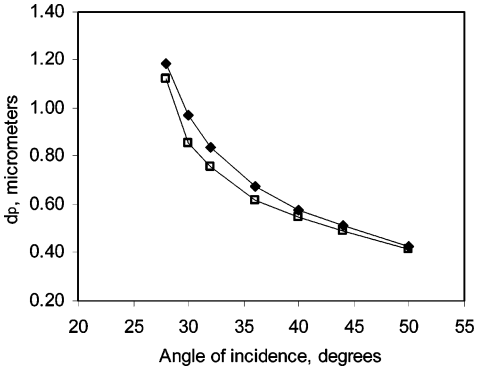

Figure 5. Depth of penetration at 1370 cm^{-1} as a function of angle of incidence: (◆) d_p into a hypothetical nonabsorbing medium of constant refractive index $n_2 = 1.60$, n_1 is 4.0; (□) modulus of d_p for PET-T calculated using the complex refractive index values obtained from Kramers−Kronig analysis.

In Figure 5, the modulus of d_p at a single wavelength (1370 cm^{-1}) is plotted as a function of angle of incidence for both the nonabsorbing medium and PET-T. The depth of penetration into PET-T is lower than the depth of penetration into the hypothetical nonabsorbing medium for all angles of incidence. The differences in d_p for the two media are however small, which shows that indeed for absorption bands of low intensity the use of d_p estimates based on a constant real refractive index is justified. We have therefore omitted the calculation of $|d_p|$ in later ATR-IR work on nominally uniaxially planar drawn PET films.

The conformational analysis of PET requires the calculation of the intensity weight coefficients of two related *trans* and *gauche* absorption bands. For that purpose a calibration curve (Figure 6) was constructed in accord with (2) using absorption coefficient data (K_0) derived from the ATR-IR spectra of PET-T and of amorphous PET films drawn in-house on an Instron machine. The calculated weight coefficients are $a_{trans} = 0.51$ and $b_{gauche} = 2.02$, and the parameters of linear regression are summarized in Table 2. As seen from the table the coefficient of determination R is close to unity, which indicates that the regression curve fits well the experimental data. In addition, the F-statistic of regression is much greater than the table value (F_T). The regression is therefore significant, and the obtained coefficients a_{trans} and b_{gauche} can be used for concentration analysis.

The *trans*/*gauche* content of PET-T for each depth of penetration was determined in accord with eq 1. The

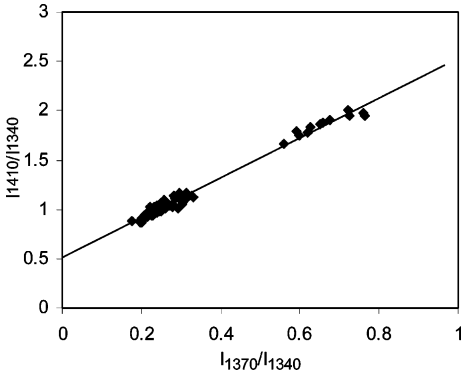

Figure 6. *Trans/gauche* calibration curve of PET: ◆, experimental points; solid line, linear regression curve.

Table 2. Parameters of the Linear Regression Fit of Figure 6[a]

observations	90
intercept (a_{trans})	0.512
x-variable (b_{gauche})	2.020
R^2	0.986
$F(\alpha = 0.05, \nu_1 = 1, \nu_2 = 88)$	6088
$F_T(\alpha = 0.05, \nu_1 = 1, \nu_2 = 90)$	3.95

[a] R = coefficient of determination; F-statistic: F = observed value, F_T = table value; α = level of significance; ν_1 = degrees of freedom (regression); ν_2 = degrees of freedom (residual).

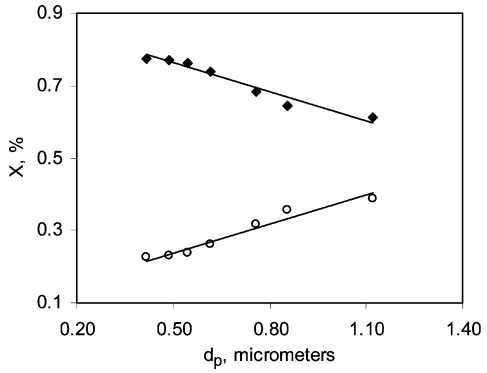

Figure 7. *Trans/gauche* concentration in PET-T as a function of depth of penetration: ◆, *trans* conformer concentration; ○, *gauche* conformer concentration.

obtained *trans/gauche* estimates were further normalized to 100%, and their values are plotted as a function of depth of penetration in Figure 7. The *trans*-EG conformer content of PET-T changes from ca. 78% at $d_p = 0.4$ μm to ca. 61% at 1.1 μm. In the figure, the structural changes are emphasized by a linear fit to the data, but this is not an attempt to predict the shape of the concentration profile. The true profile can be revealed only with the use of additional calculations based on the theory of wave propagation in stratified media. As evident from Figure 7, there is a clear trend of decrease in *trans*-PET concentration with distance from the film surface. Because of the correlation between the degree of crystallinity and the *trans* conformer content in PET, it is plausible to assume that the trend also signifies a change in the surface degree of crystallinity of PET-T.

We have previously shown, using noncontact AFM of biaxially drawn PET films, that their surface is densely populated by topographic features, approximately 20–40 nm long and wide.[33] Since amorphous PET is featureless we suggested that these features represent crystallites formed during drawing. The high *trans*-EG concentration at the smallest depth of penetration obtained from the ATR-IR analysis of PET-T correlates well with the high area coverage by crystallites in the AFM images of biaxially drawn PET films. Such a correlation gives credibility to the X_{trans} values of Figure 7.

For PET-T, the degree of crystallinity calculated on the basis of three DSC measurements is 40.1 ± 1.8%. The latter result combined with the decrease in *trans* conformer concentration at the greater depths of penetration in Figure 7 implies that the surface of PET-T possesses a greater degree of structural order than its bulk.

Analysis of Molecular Orientation. Order has an additional element to the microscopic arrangement of structural units—their macroscopic orientation. It is therefore pertinent to examine how chain orientation in PET-T varies with distance from its surface. Qualitative information about chain orientation can be obtained using the so-called dichroic ratios D defined as the ratios of the principal absorptions A_i ($i = x, y, z$) at a particular wavenumber of the optically anisotropic material.[32] The use of dichroic ratios in the depth-profiling ATR-IR analysis of a stratified medium is convenient because they are not affected by the wavelength dependence of d_p.

Figure 8a,b shows the dichroic ratios of the 1340 and 971 cm^{-1} *trans*-ethylene glycol bands. The $D_{x/z}$ and $D_{y/z}$ ratios of both absorptions decrease with distance from the film surface. This suggests that there is an overall improvement in orientation in this region. In particular, since the changes are observed in the values of the in-plane/out-of-plane ratios, these results can be tentatively interpreted as evidence for improvement in the in-plane orientation of the *trans*-ethylene glycol conformer at the film surface. A similar improvement in in-plane orientation at the smaller depths of penetration is suggested for the benzene ring unit of PET by the dichroic ratio data for the 1019 cm^{-1} absorption (Figure 8c). In Figure 8d, we have plotted $D_{z/x}$ and $D_{z/y}$ instead of $D_{x/z}$ and $D_{y/z}$ for the 875 cm^{-1} out-of-plane deformation. While due to the large data spread it cannot be confirmed with certainty, it seems that the two ratios tend to decrease toward the smaller depths of penetration. Such a decrease is in line with the indication of an improvement in in-plane orientation provided by the dichroic ratios of the other three absorptions.

The overall picture obtained using dichroic ratios appears rather consistent. The results however must be treated with caution. Notably, the increase in $D_{x/z}$ and $D_{y/z}$ in Figure 8a–c is due to the decrease of k_z at the smaller depths of penetration. In the figure, this is evidenced by the similar rate of change of the dichroic ratios. Because of the high level of molecular orientation in PET-T, the intensity of bands in the k_z spectrum is very weak for vibrations, the transition dipole moment of which lies predominantly along the chain axis. For example, in our experimental data it varies between 0.065 and 0.039 for the 1340 cm^{-1} band. For such low intensities the band shape in the derived k_z spectra is frequently very poorly defined and is easily affected by the choice of baseline points. It is therefore difficult to make a distinction between a true structural change and a systematic variation due to experimental Kramers–Kronig calculation and data handling errors.

We have data similar to that presented in Figure 8 for 12 more films, both sides of which were analyzed

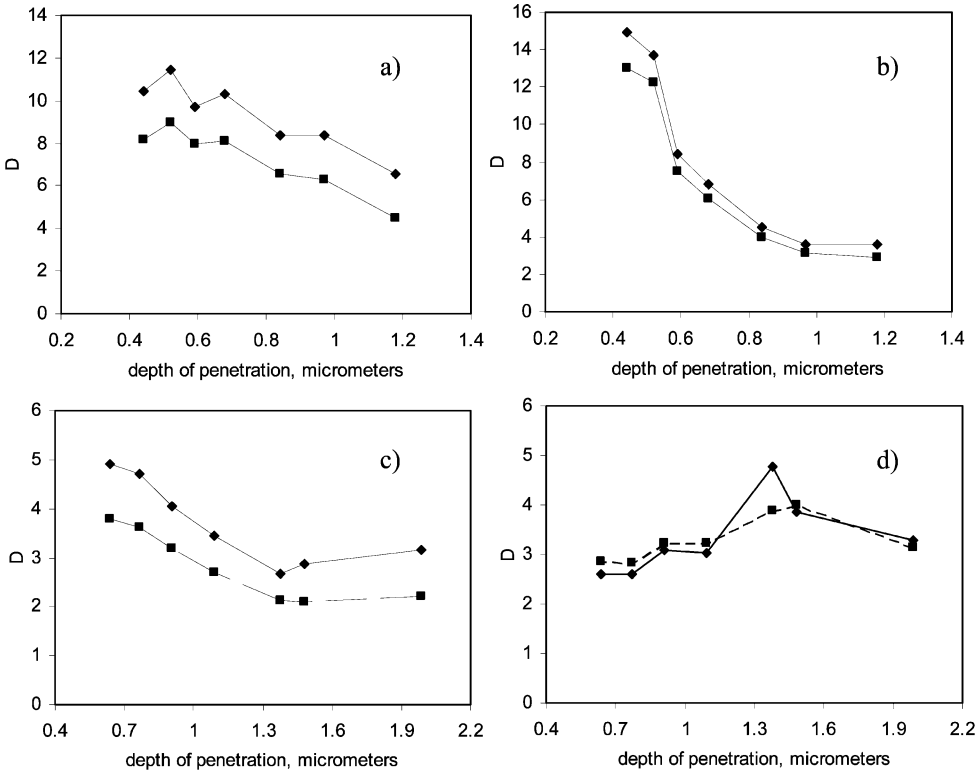

Figure 8. Depth profiling analysis of PET-T using the dichroic ratios (D) of absorption index band intensities. *trans*-EG orientation: (a) 1340 cm^{-1}; (b) 971 cm^{-1}; benzene ring orientation; (c) 1019 cm^{-1}; (d) 875 cm^{-1}. Symbols: (a–c) ◆, $D_{x/z}$; ■, $D_{y/z}$; (d) ◆, $D_{z/x}$; ■, $D_{z/y}$.

using ATR-IR spectroscopy.[34] The results show that the use of dichroic ratios of absorption index band intensities is capable of revealing differences in molecular orientation between the two sides of a film and their change as a result of thermomechanical treatment. Some characteristic differences are also present in the actual dichroic ratio depth profiles of films with different thermomechanical history. Our overall conclusion, however, is that the data are not of a good enough quality to unequivocally prove the existence of orientation gradients.

In principle, a much more detailed picture of the orientation of the *trans*-PET conformer can be obtained following the quantitative approach for infrared orientational analysis outlined in the Methodology section. The application of the latter to the ATR-IR analysis of a stratified medium, however, has its own shortcoming. We recall that for a film with a general biaxial statistical symmetry in its structure it is necessary to calculate four orientation average coefficients P_{lmn} using the $n-k$ parameters of two absorption bands belonging to a particular functional group.[25] The involvement of two absorption bands in the analysis inevitably poses some ambiguity in the depth profiling of stratified media due to the fact that for vibrations with sufficient wavenumber separation the depth of penetration at each absorption peak maximum would be rather different.

Figure 9a shows the variation of $|d_p|$ with angle of incidence for the two *trans*-EG vibrations (1340 and 971 cm^{-1}) used earlier for qualitative assessment of orientation. The depth of penetration at 1340 cm^{-1} is smaller than the depth of penetration at 971 cm^{-1}. In addition, the difference in $|d_p|$ varies from 0.2 to 1.0 μm as the angle of incidence decreases. For the 1019 and 875 cm^{-1} benzene ring vibrations the calculated $|d_p|$ difference is smaller—it changes from 0.04 to 0.62 μm (Figure 10b).

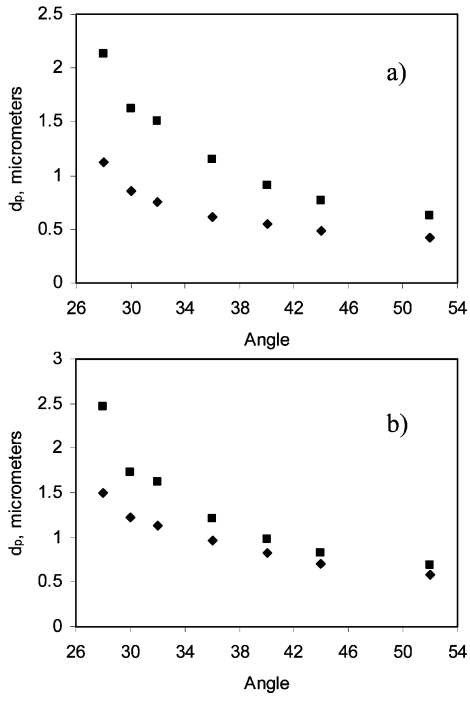

Figure 9. Estimates of $|d_p|$ as a function of angle of incidence obtained for the following absorption bands: (a) ■, 1340 cm^{-1}; ◆, 971 cm^{-1}; (b) ■, 1019 cm^{-1}; ◆, 875 cm^{-1}.

Hence, when using a simplified optical model for extraction of optical constants, the employment of the quantitative approach for orientational analysis is more favorable at the greater angles of incidence due to the smaller differences in d_p.

Alternatively, k-spectrum band intensities derived from measurements at different angles of incidence can be used in order to utilize data arising from similar

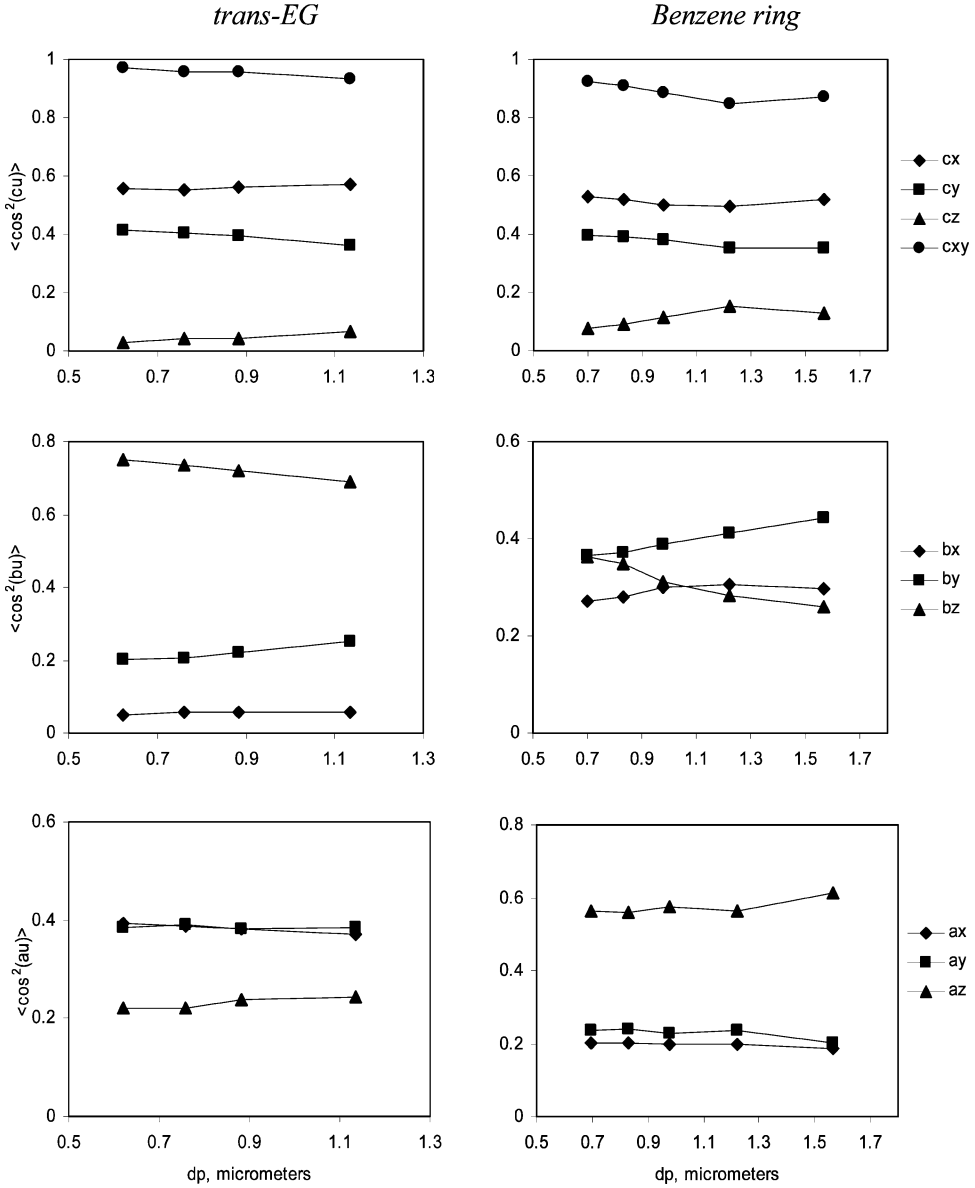

Figure 10. *trans*-EG and benzene ring orientation in PET-T with respect to the *Oxyz* coordinate system calculated using data sets based on d_p matching: top row, *c*-axis orientation; middle row, *b*-axis orientation; bottom row, *a*-axis orientation. The sum of $\langle\cos^2(cx)\rangle$ and $\langle\cos^2(cy)\rangle$ is denoted as $\langle\cos^2(cxy)\rangle$ in the top figure row.

Table 3. Depth of Penetration Matching for the 1340 and 971 cm^{-1} Absorption Bands of PET

AOI_{1340}, deg	d_p^{1340}, μm	d_p^{971}, μm	AOI_{971}, deg
28	1.12	1.15	36
30	0.85	0.91	40
32	0.75	0.76	44
36	0.62	0.63	52

depths of penetration. As shown in Table 3, on the basis of d_p the data for the two *trans* bands can be combined in four sets. For the 1019 and 875 cm^{-1} benzene ring vibrations, the data can be arranged in five sets.

Figure 10 presents the orientation of the *trans*-EG conformer (left column) and of the benzene ring (right-hand side column) of the PET monomer unit with respect to the macroscopic directions *x*, *y*, *z* in the form of averaged squared direction cosines. The data are plotted against the $|d_p|$ averages for the two groups of absorption bands.

In the top row of Figure 10, the cosines $\langle\cos^2(cx)\rangle$ and $\langle\cos^2(cy)\rangle$ are substantially greater than $^1/_3$ for both groups, whereas the averaged $\langle\cos^2(cz)\rangle$ is 0.05 for the *trans*-EG conformer and 0.11 for the benzene ring. These results show that the long axes of the PET monomer unit are oriented predominantly along the two drawing directions and lie within the film plane. The extent of this orientation is further emphasized by the sum of the two in-plane cosines $\langle\cos^2(cxy)\rangle$.

The middle and bottom rows of Figure 10 contain the cosines $\langle\cos^2(bu)\rangle$ and $\langle\cos^2(au)\rangle$ ($u = x, y, z$), which provide information about the rotational orientation of the functional groups. Here, however, we have come to a major contradiction in the obtained results. As evident from the figure, $\langle\cos^2(bz)\rangle$ for the *trans*-EG conformer is in the range 0.69−0.75; $\langle\cos^2(az)\rangle$ is correspondingly lower, 0.24−0.22. This indicates that the *trans*-EG unit is preferentially rotated out of the film plane; e.g., the *Obc* plane of the unit is predominantly aligned along the normal to the PET-T film plane. In the same figure, however, $\langle\cos^2(bz)\rangle$ for the benzene ring varies between 0.22 and 0.36, and $\langle\cos^2(az)\rangle$ varies from 0.61 to 0.56. This suggests that the *Obc* plane of the benzene ring is predominantly oriented within the film plane.

It is unlikely that the obtained difference in orientation represents truly the surface structure of PET-T. Since the PET film is predominantly crystalline and the polymer in its crystalline form is in an *all-trans* conformation, both the ethylene glycol and the benzene ring units should have the same type of orientation. Previous XRD analyses of PET films subjected to uniaxial planar deformation have shown that the benzene ring planes become highly oriented within the film plane.[35,36] We therefore consider our analysis for the benzene ring orientation credible.

The difference in the type of rotational orientation obtained for the *trans*-EG unit might be accounted for by miscalculation of the angles between the transition dipole moments of the two ethylene glycol group vibrations and the molecular chain axis (Table 1). This issue would certainly have to be followed further in order to find the reason for the discrepancy.

Conclusions

The quantitative ATR-IR analysis of a commercial PET film (PET-T) has shown that the concentration of the *trans*-ethylene glycol conformer in PET-T increases substantially on approach to the film surface. According to our calculations, the *trans* conformer content changes from 77% at a depth of penetration 0.4 μm to 61% at a depth of penetration of 1.1 μm. Since there is a well-established correlation between the *trans*-EG concentration and the degree of crystallinity in PET, this result implies that the surface degree of crystallinity of PET-T is greater than that of the film bulk.

We have reviewed the application of the technique in the orientational depth profiling of anisotropic PET films. Depth profiling using dichroic ratios is convenient because the intensities of only one absorption band are utilized. The quantitative analysis of molecular orientation is further complicated by the involvement in the analysis of the optical constants of two absorption bands.

The orientational analysis of PET-T using averaged squared direction cosines has shown that the long axes of both the *trans*-EG and the benzene ring units of PET are oriented predominantly along the two drawing directions of the film. A high degree of in-plane orientation was found for the benzene ring in accord with previous studies,[35,36] but an out-of-plane orientation was obtained for the *trans*-EG segment. The origin of this discrepancy is not clear and needs to be investigated further.

We have been unable to confirm the presence of chain orientation gradients in PET-T. The difficulty in applying orientational depth profiling to highly anisotropic films stems from the low intensity of the optical constant spectra along the direction of no preferential chain orientation. For polymer films this is the film thickness direction. Since the (n_z, k_z) data are derived from the p-polarized light reflectivity spectrum of the film using the in-plane optical constants,[1] they bear the errors of two experimental measurements and calculation procedures instead of one. The success of orientational depth profiling would therefore critically depend on minimizing all experimental errors in order to determine more accurately the out-of-plane optical constant spectra. This in turn implies performing the ATR-IR experiments under very stringent conditions: complete light polarization, little or no angular spread of the incident light, accurate alignment of the light polarization direction with the optical axes of the film, and the acquisition of reflectivity spectra of uncompromisingly good quality void of baseline distortion.

Acknowledgment. The authors thank the Toppan Printing Co. Ltd., Japan, for providing the financial support for this work.

References and Notes

(1) Kirov, K. R.; Assender, H. E. *Macromolecules* **2004**, *3*, 894.
(2) Werner, E.; Janocha, S.; Hopper, M. J.; Mackenzie, K. J. In *Encyclopaedia of Polymer Science and Engineering*, 2nd ed.; Mark, H. F., Bikales, N. M., Overberger, C. G., Menges, G., Eds.; John Wiley and Sons: New York, 1988; Vol. 12, p 193.
(3) Kwon, S. H.; Paik, S. Y.; Yoo, J. S. *Synth. Met.* **2002**, *30*, 55.
(4) Herrero, J.; Guillén, C. *Vacuum* **2002**, *67*, 611.
(5) Quintanilla, L.; Rodriguez-Cabello, J. C.; Jahwari, T.; Pastor, J. M. *Polymer* **1993**, *34*, 3787.
(6) Fernandez, M. R.; Merino, J. C.; Pastor, J. M. *Polym. Eng. Sci.* **2000**, *40*, 95.
(7) Hayes, N. W.; Beamson, G.; Clark, D. T.; Law, D. S.-L.; Raval, R. *Surf. Interface Anal.* **1996**, *24*, 723.
(8) Keddie, J. L.; Jones, R. A. L.; Cory, R. A. *Europhys. Lett.* **1994**, *27*, 59.
(9) Everall, N.; Davis, K.; Owen, H.; Pelletier, M. J.; Slater, J. *Appl. Spectrosc.* **1996**, *50*, 388.
(10) Walls, D. J.; Coburn, J. C. *J. Polym. Sci., Polym. Phys.* **1992**, *30*, 887.
(11) Cole, K. C.; Daly, H. B.; Sanschagrin, B.; Nguyen, K. T.; Ajii, A. *Polymer* **1999**, *40*, 3505.
(12) Grime, D.; Ward, I. M. *Trans. Faraday Soc.* **1958**, *54*, 959.
(13) Ward, I. M.; Wilding, M. A. *Polymer* **1977**, *18*, 327.
(14) Lapersonne, P.; Bower, D. I.; Ward, I. M. *Polymer* **1992**, *33*, 1277.
(15) Imai, M.; Mori, K.; Mizukami, T.; Kaji, K.; Kanaya, T. *Polymer* **1992**, *33*, 4451.
(16) Imai, M.; Mori, K.; Mizukami, T.; Kaji, K.; Kanaya, T. *Polymer* **1992**, *33*, 4457.
(17) Imai, M.; Kaji, K.; Kanaya, T. *Macromolecules* **1994**, *27*, 7103.
(18) Imai, M.; Kaji, K.; Kanaya, T.; Sakai, Y. *Phys. Rev. B* **1995**, *52*, 12696.
(19) Ryan, A.; Fairclough, J. P. A.; Terrill, N. J.; Olmsted, P. D.; Poon, W. C. K. *Faraday Discuss.* **1999**, *112*, 13.
(20) Mahendrasingam, A.; Martin, C.; Fuller, W.; Blundell, D. J.; Oldman, R. J.; MacKerron, D. H.; Harvie, J. L.; Riekel, C. *Polymer* **2000**, *41*, 1217.
(21) Welsh, G. E.; Blundell, D, J.; Windle, A. H. *J. Mater. Sci.* **2000**, *35*, 5225.
(22) Cunningham, A.; Davies, G. R.; Ward, I. M. *Polymer* **1974**, *15*, 743.
(23) Jarvis, D. A.; Hutchinson, I. J.; Bower, D. I.; Ward, I. M. *Polymer* **1980**, *21*, 41.
(24) Roe, R.-J. *J. Appl. Phys.* **1964**, *36*, 2024.
(25) Ward, I. M. *Adv. Polym. Sci.* **1985**, *66*, 81−115.
(26) Daubenny, R. P.; Bunn, C. W. *Proc. R. Soc. London* **1956**, *A226*, 531.
(27) Nicholson, T. M.; Davies, G. R.; Ward, I. M. *Polymer* **1994**, *35*, 4259.
(28) Cail, J. I.; Stepto, R. F. T.; Taylor, D. J. R.; Jones, R. A.; Ward, I. M. *Phys. Chem. Chem. Phys.* **2000**, *2*, 4361.
(29) Mark, J. E., Ed.; *Polymer Data Handbook*; Oxford University Press: New York, 1999; pp 558−560.
(30) Harrick, N. J. *Internal Reflection Spectroscopy*; Interscience Publishers: New York, 1967.
(31) Mirabella, F. M., Jr. *J. Polym. Sci., Polym. Phys.* **1983**, *21*, 2403.
(32) Zbinden, R. *Infrared Spectroscopy of High Polymers*; Academic Press: New York, 1964.
(33) Dinelli, F. Assender, H. E.; Kirov, K.; Kolosov, O. V. *Polymer* **2000**, *41*, 4285.
(34) Kirov, K. R.; Assender, H. E.; Quantitative ATR-IR Analysis of Anisotropic Polymer Films: Surface Structure Development in PET upon Drawing. Manuscript in preparation.
(35) Lapersonne, P.; Tassin, J. F.; Monnerie, L.; Beautemps, J. *Polymer* **1991**, *32*, 3331.
(36) De Champchesnel, J. B. F.; Tassin, J. F.; Bower, D. I.; Ward, I. M.; Lorentz, G. *Polymer* **1994**, *35*, 4092.
(37) Spiby, P.; O'Neill, M. A. O.; Duckett, R. A.; Ward, I. M. *Polymer* **1992**, *33*, 4479.
(38) Liang, C. Y.; Krimm, S. *J. Mol. Spectrosc.* **1959**, *3*, 554.
(39) Cunningham, A.; Ward, I. M.; Willis, H. A.; Zichy, V. *Polymer* **1974**, *15*, 749.

MA050495I